

TWO COMPONENT EMDEN SPHERE

H.V. CAPELATO*

Centre d'Etudes Nucléaires de Saclay, Gif-sur-Yvette, France

D. GERBAL and E. SALVADOR SOLE

Groupe d'Astrophysique Relativiste, Observatoire de Meudon, France

G. MATHEZ and A. MAZURE

Laboratoire d'Astrophysique Théorique, Observatoire de Meudon, Université de Paris VII, France
and

J. ROLAND

Observatoire de Meudon, France

We give the theory of a self gravitational gas sphere. The gravitational field is generated by two components, each of them being independently an isothermal gas. Various quantities of interest as density profiles, core radii of both components, masses, free-free luminosity, surface brightness, central surface density, overestimate of central mass density are given for different values of both parameters which arise naturally (ratio of central densities, ratio of rms velocities).

Fundamental changes appear when compared with a theory in which the second component is a "test component". Procedures are given for the complete analysis of real astrophysical configurations such as clusters of galaxies or globular clusters.

Key words: stellar systems – galaxies – clusters of galaxies

1. INTRODUCTION

The theory of the Emden gravitational isothermal gas sphere (confined in a finite shell) was established as early as 1902 (see Zwicky 1957 p. 134). The results of this theory are still applied by many authors to the analysis of clusters of stars (globular clusters; nuclei of galaxies) or of galaxies. From observational data such as density profile, core radius and velocity dispersion, are deduced various quantities as the central mass density and the dynamical mass.

Emden's theory assumes that the gravitational field is generated by a single distribution of molecules, stars, or galaxies. Nevertheless a mixture of various phases is found in most astrophysical objects. For instance:

1. The discovery of a very hot gas responsible for thermal X-ray emission shows the presence, in clusters of galaxies (Forman *et al.* 1972), of an invisible second component. It is interesting to note that the mass of this gas has been estimated, in some cases, to be of the order of the visible mass of galaxies (Bahcall 1977).
2. In globular clusters are found two populations of stars (red giants and white dwarfs).
3. One (or more) gaseous phase coexists in galaxies or nuclei of galaxies with the distribution of stars.
4. A massive halo of small invisible stars has been sometimes assumed to exist in spiral galaxies, so that the visible stars constitute only a small fraction of the total galaxy.

It appears therefore useful to study the theory of the two-component gravitational gas sphere and the purpose of the present paper is to take into account the gravitational effects of the invisible component.

It seems indeed to us somewhat incorrect to neglect them by considering simply the invisible component as a "test-component" in hydrostatic equilibrium with the gravitational potential generated uniquely by the visible component. The latter model, hereafter referred to as TC model, has been used by many authors: Lea (1975), Gull and Northover (1975), Cavaliere and Fusco-Femiano (1976), Sarazin and Bahcall (1977).

On the contrary we show in this paper that the TC model is, according to the case, either a good or a bad approximation. The dynamical influence of the invisible component may be discernible through its effects upon the density profile of the visible component. We show how, according to the model, the central density, the mass of the core and other dynamical quantities are related to observable quantities and how their values depend strongly on the free parameters of the problem which are the ratio η of both central densities and the ratio α of both temperatures. Furthermore, we attempt to answer the following

* On leave of absence from Instituto Astronômico e Geofísico, Universidade de São Paulo, Brazil.

problem: from how many observations and what observations and how is it possible to deduce all the various characteristics of a configuration (globular cluster, cluster of galaxies...) accounting for both the visible and the invisible components which constitute it.

In section 2 are given the basic equations; in section 3 are studied the asymptotic behaviours of both the density and the free-free surface brightness profiles. In section 4 we look for the theoretical quantities which allow the easiest comparisons with data. Results are given in section 5.

2. EQUATIONS

The gravitation potential $U(r)$ obeys Poisson's equation:

$$\Delta U(r) = 4\pi G [\rho_a(r) + \rho_b(r)] \quad (1)$$

$\rho_a(r)$ and $\rho_b(r)$ are the mass distributions of both the visible a -component and the invisible b -component.

We assume both components to be without interaction other than gravitational, each of them being in equilibrium with the gravitation potential U . It follows that:

$$\rho_i(r) = \rho_i(0) \exp[-3 U(r)/v_i^2]; \quad i = a, b \quad (2)$$

v_i being the three dimensional velocity dispersion of the i -particles. The potential U is chosen to be zero at origin: $U(0) = 0$. By using as new function:

$$\psi(r) = 3 U(r)/v_a^2$$

and introducing:

$$\eta = \rho_b(0)/\rho_a(0); \quad \alpha = v_b^2/v_a^2$$

equation (1) reads:

$$\Delta \psi(s) = e^{-\psi(s)} + \eta e^{-\psi(s)/\alpha} \quad (3)$$

where we use as new length unit the structural index β defined by:

$$\beta^{-2} = 12 \pi G \rho_a(0)/v_a^2; \quad r = \beta s$$

and as "dimensionless mass densities":

$$\rho_i^* = \rho_i(\beta s)/\rho_a(0); \quad i = a, b.$$

Note that the choice of β is related to the characteristics ($\rho_a(0)$ and v_a^2) of the first component; it has been chosen in order to compare our results to observations, since the a -component is assumed to be the visible component.

For discussing equations and results, it is preferable to introduce dimensionless quantities such as both dimensionless masses defined in the sphere of (dimensionless) radius s :

$$M_i^*(s) = \int_0^s 4\pi s'^2 \rho_i^*(s') ds'; \quad i = a, b. \quad (4)$$

If we consider the case where the b -component is a free-free emitting gas, the total free-free emission of a fully ionized cosmic plasma (Allen 1976, p. 103) writes using the quantities defined above:

$$E_{ff} = 1.0 \times 10^{29} V_{los}^5 E_{ff}^*/\beta^4 \text{ erg } s^{-1} \text{ cm}^{-3} \quad (5)$$

where $E_{ff}^*(s) = \alpha^{1/2} [\rho_b^*(s)]^2$ is the dimensionless emissivity and V_{los} is the line-of-sight velocity dispersion of the visible particles: $V_{los}^2 = v_a^2/3$. The free-free luminosity L_{ff} is obtained by integration over volume:

$$L_{ff} = 2 \times 10^{45} (V_{los}/1000 \text{ km } s^{-1})^5 (0.25 \text{ Mpc}/\beta) L_{ff}^* \text{ erg } s^{-1} \quad (6)$$

where: $L_{ff}^* = \alpha^{1/2} \eta^2 \int e^{-2\psi/\alpha} 4\pi s^2 ds$.

* Note that α in Equation (3) is the same as $1/\beta$ in Sarazin and Bahcall (1977) or as $1/\tau$ in Cavaliere and Fusco-Femiano (1976).

As a matter of fact, most quantities of astrophysical interest are the projections on the sky of the quantities above. Let us use s and ℓ as respective arguments of 3- and 2-dimensional quantities. Both projected densities are, for instance, given by:

$$\sigma_i^*(\ell) = \int_{-\infty}^{+\infty} n_i^* (\sqrt{z^2 + \ell^2}) dz \quad (7)$$

where n_i^* are dimensionless number densities.

Similarly, the dimensionless surface brightness corresponding to free-free emission of the b -component writes:

$$B_{ff}^*(\ell) = \frac{1}{4\pi} \int_{-\infty}^{+\infty} E_{ff}^* (\sqrt{z^2 + \ell^2}) dz \quad (8)$$

The global quantities of interest are the respective total masses in the cylinder of radius ℓ :

$$M_i^*(\ell) = 2\pi \int_0^\ell d\ell' \ell' \int_{-\infty}^{+\infty} dz \rho_i^* (\sqrt{z^2 + \ell'^2}) \quad (9)$$

$$M^*(\ell) = M_a^*(\ell) + M_b^*(\ell). \quad (10)$$

All the dimensionless quantities defined above are given in terms of the potential ψ . The latter is governed by Equation (3) which depends on two parameters α and η .

3. ASYMPTOTIC BEHAVIOURS

Let us now study the asymptotic behaviours towards infinite s and ℓ of $n_i^*(s)$, $\sigma_i^*(\ell)$, $E_{ff}^*(s)$ and $B_{ff}^*(\ell)$, the expressions of which are given above.

First case: $\alpha < 1$. Towards large s , Equation (3) reduces to the single component Emden's equation. Therefore the logarithmic slopes of $n_a(s)$ and $\sigma_a(\ell)$ are -2 and -1 respectively, independently of η . The asymptotic logarithmic slopes of $\rho_b^*(s)$, $\sigma_b^*(\ell)$, $E_{ff}^*(s)$ and $B_{ff}^*(\ell)$ are then respectively: $-2/\alpha$, $1-2/\alpha$, $-4/\alpha$ and $1-4/\alpha$.

Second case: $\alpha > 1$. After a change of variable: $s = (\alpha/\eta)^{1/2} s'$ and of function: $\psi = \alpha\psi'$ equation (3) reduces again to a single component Emden's equation. The logarithmic slope of $\rho_b^*(s')$ and therefore that of $\rho_b^*(s)$ is thus -2 independently of η . The logarithmic slopes of the free-free emissivity and surface brightness are -4 and -3 respectively. On the other hand, for the a -component the slopes of $n_a^*(s)$ and $\sigma_a^*(\ell)$ are respectively -2α and $1-2\alpha$.

We can now easily study the asymptotic behaviour of a test gas in the gravitation field generated by the a -component only. In this case, Equation (3) reduces indeed exactly to Emden's equation. The relation $\rho_b^*(s) = \eta [\rho_a^*(s)]^{1/\alpha}$ (given for the central part of galaxy clusters by Cavaliere and Fusco-Femiano, 1976) holds whatever be α and the slopes of n_b and σ_b are $-2/\alpha$ and $1-2/\alpha$, that of E_{ff} and B_{ff} being $-4/\alpha$ and $1-4/\alpha$.

Table 1 summarizes the conclusions of this section. The difference between TC model and ours is remarkable in the case $\alpha > 1$ (compare rows 3 and 4, 5 and 6, 7 and 8). Note that the test component obeys the law given by Cavaliere and Fusco-Femiano, whereas the real gas obeys it in certain conditions (see table 1).

4. DYNAMICAL STUDY OF A TWO-COMPONENT CONFIGURATION

We are now in position to integrate numerically Equation (3) and to get the potential and all quantities of interest. Before doing that, we determine in this section what quantities may be useful in the study of a given astrophysical configuration. Many authors have shown, in the frame of Emden's theory, how to pass from observational data to the dynamical quantities of clusters. Zwicky (1957, pp. 138-144) has given some very good examples. Let us merely recall that from three observables which are the core radius r_c ,

the rms line of sight velocity V_{los} and the central projected density $\sigma(0)$, one can extract two dynamical quantities, the mass – and number – central densities respectively:

$$\rho(0) = \left(\frac{\ell_c}{r_c}\right)^2 \frac{V_{\text{los}}^2}{4\pi G} \quad (11)$$

$$\eta(0) = \frac{\ell_c}{r_c} \frac{\sigma(0)}{\sigma_0^*} \quad (12)$$

Note that these equations are identical to Equations (101) and (96) of Zwicky (1957) since ℓ_c is the dimensionless core-radius and r_c/ℓ_c the structural index β . σ_0^* is the dimensionless central projected density. ℓ_c and σ_0^* are respectively equal to 3.0 and 6.1 in the single-component Emden's sphere theory.

From $\rho(0)$ and $n(0)$ may be inferred: i) the dynamical mass of the core which is usually approximated by:

$$M_c \approx \rho(0) \frac{4\pi}{3} r_c^3 \quad (13)$$

and ii) the dynamical mass of an individual particle, equal to the ratio of the central mass density to the central number density:

$$m = \rho(0)/n(0) \quad (14)$$

Let us show, now, how to determine the dynamical quantities from observational data in the frame of the two-component theory. α is known either from asymptotic profiles or from the observed v_a^2 and v_b^2 (or T_b).^{*} Once α is known, η is obtained by comparing the observed $r_{\text{cb}}/r_{\text{ca}}$ (or $r_{\text{ff}}/r_{\text{ca}}$), r_{ff} being the radius where the surface brightness is one-half of its central value, to the corresponding theoretical families of ratios $\ell_{\text{cb}}/\ell_{\text{ca}}$ (α, η) (or $\ell_{\text{ff}}/\ell_{\text{ca}}$ (α, η)) obtained by integration of Equation (3) and projection.

Equations (11) and (12) still hold for the visible component, but we have here $\ell_c = \ell_{\text{ca}}$ (α, η) and $\sigma_0^* = \sigma_0^*$ (α, η). They allow, therefore, to calculate $\rho_a(0)$, $\rho_b(0) = \eta \rho_a(0)$, $\rho(0) = (1 + \eta) \rho_a(0)$, and $n_a(0)$. Equations (13) and (14) give then the dynamical masses:

$$M_c = (1 + \eta) \ell_{\text{ca}}^2 r_{\text{ca}} \frac{V_{\text{los}}^2}{3G} \quad (15)$$

$$m_a = \frac{\ell_{\text{ca}}}{r_{\text{ca}}} \frac{\sigma_0^*}{\sigma(0)} \frac{V_{\text{los}}^2}{4\pi G} \quad (16)$$

All the dynamical masses defined above are generally proportional to the central density which is evaluated from data through Equation (11). It is interesting to introduce the ratio R of the central densities found from the same data in the respective frames of the single – and of the two – component theories. From Equation (11) one gets:

$$R = \left[\frac{9 V_{\text{los}}^2}{4\pi G r_{\text{ca}}^2} \right] / \left[\frac{(1 + \eta) V_{\text{los}}^2}{4\pi G} \left(\frac{\ell_{\text{ca}}}{r_{\text{ca}}} \right)^2 \right] = \frac{9}{(1 + \eta) \ell_{\text{ca}}^2} \quad (18)$$

Note that the ratio of the central densities of the *visible* component found in both theories is:

$$R_a = (1 + \eta)R = 9/\ell_{\text{ca}}^2 \quad (19)$$

R and R_a are given in Table 3 (columns 12 to 21).

An alternative value of the dynamical mass – theoretically more correct – given by Equation (11), may be calculated by integration of Equation (3). In Table 6 (columns 2 to 6) is given the dimensionless mass of the *a*-component in the cylinder of radius ℓ_{ca} . It should be noticed that this mass which is equal to 110

^{*} In the case of globular clusters, v_b^2 is not observed, and α remains therefore unknown.

for ($\alpha=0.25$; $\eta=0.1$) is equal to only 1.1 for ($\eta=10$; $\alpha=16$). This indicates a strong concentration of the visible component when α is high, i.e. when the velocity dispersion of the invisible particles is greater than that of the visible ones.

5. RESULTS

All calculations were performed by numerical integration of Equation (3). In Table 2 are determined the values to be given to η and α in the various applications listed in section 1. Because of its weight in the exponential factor α has only been varied around unity.

5.1 Visible component

The visible density profiles $\sigma_a(\ell)/\sigma_{0a}$ are given in figures 1 to 5. The various asymptotic behaviours correspond well to the results of section 3. The relation between α and the asymptotic slope is a remarkable dynamical effect, independent of η (see section 3).

The values of ℓ_{ca} and σ_{0a}^* are given in columns 2 to 11 of table 3. Note that towards small α ℓ_{ca} tends to Emden's value: $\ell_c=3.0$ independently of η . On the other hand, towards high values of α , the limits of ℓ_{ca} are in the range [0.6-2.3], indicates a more pronounced concentration of the visible component with respect to the single component Emden profile.

5.2. Invisible component

Depending on the physical nature of the invisible component two points of view are possible. The invisible mass density which appears in Equation (3) may, as already shown, correspond to a gas of stars as well as of protons. In particular, some people believe that very small stars around $0.1 M_\odot$ (so-called population III) constitute massive halos of galaxies and fill clusters of galaxies (White 1977; Gunn 1978) and globular clusters.

In this case one will be concerned with density profiles. On the other hand, if the invisible gas is a proton gas responsible for free-free emission in clusters of galaxies surface brightness profiles will be needed.

In figures 6 to 10 are given density profiles $\sigma_b(\ell)/\sigma_{0b}$, versus radius in units of visible core radius. Note that asymptotic slopes are conform to the previsions of table 1. These profiles may be verified to be very different from those obtained in the "test-component" theory (dotted curves) except for $\alpha=1$.

According to section 4 are given, in columns 2 to 6 of table 4, the ratios of both core-radii: ℓ_{cb}/ℓ_{ca} . It should be noticed that the increase of this ratio with increasing α is considerably less than in TC model (see column 7). This difference is due to the very different profiles obtained in both models for $\alpha>1$. Ratios ℓ_{ff}/ℓ_{ca} are given in columns 8 to 12 of the same table. Surface brightness profiles are given in figures 11 to 15. Here too is confirmed the asymptotic behaviour predicted in table 1. Note that the difference with the TC theory (dotted curves) is considerable. (These curves are equivalent to those given in figure 6 of Sarazin and Bahcall). The mass of intracluster gas in the sphere of radius s or in the cylinder of radius ℓ may be calculated by integration of Equation (3). In table 5, columns 2 to 6 give the mass of b -component within the sphere of radius s_{cb} , columns 7 to 11 give the ratio of masses of both components and columns 12 to 16 give the *total* free-free luminosity of the cluster.

In table 6, columns 7 to 11 are given the b -mass within the cylinder of radius ℓ_{cb} and in columns 12 to 16 the ratio M_b/M_a in the same cylinder. In figure 16 is plotted versus $\log \alpha$ the ratio of the masses of both components within the visible core.

In Appendix further results such as the potential and other quantities of interest are given versus the spherical radius.

6. CONCLUSIONS

Taking into account the gravitational effects of the second component is quite justified by the results thus obtained:

- both asymptotic density profiles a and b (we show in particular in table 1 the limit of validity of the relation given by Cavaliere and Fusco-Femiano (1976)) and the luminosity profile b are found to be different, and sometimes quite different, from those obtained in TC model. The visible component is often more concentrated than in TC model as pointed out in section 5.1;
- the usual dynamical quantities deduced from the same data are quite modified (table 3). The core radii of invisible component are generally smaller (and for large α very smaller) than core radii of TC gas (table 4). The use of a two-component theory may modify considerably the dynamical mass calculated from the same data (see table 3, Columns 12 to 21).

We estimate, therefore, that the physical conditions in both the visible and the invisible components, can be rightly determined from present and future observations only in the frame of a fully dynamical model of the kind we have exposed in this paper.

One of us (H.V.C.) acknowledges financial supports from CNPQ (Brazil).

APPENDIX

We give here the variations versus radial distance of some dimensionless quantities defined in section 2. S is the radius in units of the structural index β , Ψ is the potential, ρ_{OA} and ρ_{OB} are the respective dimensionless mass densities; M_A , M_B and $M = M_A + M_B$ are the masses, defined by Equation (4), in the sphere of radius S . Any real mass will be obtained by multiplying the corresponding dimensionless mass by a factor:

$$M_i(r)/M^*(s) = \beta^3 \rho_a(0) = \beta V_a^2 / 12\pi G$$

L_X is the free-free luminosity of the b -component, assumed to be a fully ionized cosmic gas (the definition of L_X is given in Equation (6)).

REFERENCES

- Allen, C.W.: 1976, in The Athlone Press, London (ed.), *Astrophysical Quantities*.
 Bahcall, N.: 1977, *Ann. Rev. Astron. Astrophys.* **15**, 505.
 Cavaliere, A. and Fusco-Femiano, R.: 1976, *Astron. Astrophys.* **49**, 137.
 Da Costa, G.S. and Freeman, K.C.: 1976, *Ap. J.* **206**, 128.
 Faulkner, D.J. and Freeman, K.C.: 1977, *Ap. J.* **211**, 77.
 Forman, W., Kellog, E., Gursky, H., Tanabaum, H. and Giacconi, R.: 1972, *Ap. J.* **178**, 309.
 Gull, S.F. and Northover, K.J.E.: 1975, *Monthly Notices Roy. Astron. Soc.* **173**, 585.
 Lea, S.M.: 1975, *Astrophys. Letters* **16**, 141.
 Lea, S., Silk, J.L., Kellog, E. and Murray, S.: 1973, *Ap. J. Letters* **184**, LIII.
 Mattila, K.: 1977, *Astron. Astrophys.* **60**, 425.
 Ostriker, J.P. and Peebles, P.J.B.: 1973, *Ap. J.* **186**, 467.
 Sarazin, C.L., Bahcall, J.N.: 1977, *Ap. J. Suppl.* **34**, 451.
 White, S.D.M.: 1977, *Monthly Notices Roy. Astron. Soc.* **179**, 33.
 Zwicky, F.: 1957, in Springer Verlag, Berlin (ed.), *Morphological Astronomy*.

H.V. Capelato

D. Gerbal
 E. Salvador Sole
 G. Mathez
 A. Mazure
 J. Roland

Centre d'Etudes Nucléaires de Saclay
 Gif-sur-Yvette (France)

Observatoire de Meudon
 F-92190 Meudon (France)
 * Université de Paris VII

Table 1 Asymptotic logarithmic slopes of n , σ (volume- and surface-number densities), E_{ff} and B_{ff} (free-free emissivity and surface brightness). A tilde indicates the results of TC model.

	$\alpha < 1$	$\alpha = 1$	$\alpha > 1$
η_a	-2	-2	-2α
σ_a	-1	-1	$1-2\alpha$
η_b	$-2/\alpha$	-2	-2
$\tilde{\eta}_b$	$-2/\alpha$	-2	$-2/\alpha$
σ_b	$1-2/\alpha$	-1	-1
$\tilde{\sigma}_b$	$1-2/\alpha$	-1	$1-2/\alpha$
E_{ff}	$-4/\alpha$	-4	-4
\tilde{E}_{ff}	$-4/\alpha$	-4	$-4/\alpha$
B_{ff}	$1-4/\alpha$	-3	-3
\tilde{B}_{ff}	$1-4/\alpha$	-3	$1-4/\alpha$

Table 2 Column 1 refers to the various applications considered in the introduction. Columns 2 and 3 give the a and b components, columns 4 and 5 their respective densities (in g. cm^{-3}), columns 6 and 7 crude estimates of η and α and column 8 gives the references.

Application No	Visible a component	Invisible b-component	$\rho_a(0)$	$\rho_b(0)$	η	α	References
1	Galaxies	X- gas hidden mass	10^{-26}	10^{-27} 10^{-25}	0.1 10	1 ?	Bahcall 1977
2	Giant * 90% of total luminosity.	Low mass * 10% of total luminosity	20% of total mass	80% of total mass	4	$1 \ll \alpha < 7$	Da Costa Freeman 1976
3	Visible * velocity ~ 100km/s.	Interstellar gas 100°K or 8000°K	10^{-23}	10^{-24}	0.1	10^{-2} or 10^{-4} .	Allen pp.250-251-265.
4	Visible *	Invisible *	10^{-23}	10^{-22}	10	$> 1 ?$	

Table 3 Columns 2 to 11: dimensionless core radius and projected central density σ_{a0}^* of the visible component; columns 12 to 21: R and R_a are the ratios, defined in Equations (18) and (19), of the central densities found in one- or in two-component Emden's sphere theories.

η	$1/\alpha$					σ_{a0}^*					R		R_a		R		R_a			
	1/10	1/3	1	3	10	1/10	1/3	1	3	10	1/10	1/3	1	3	10	1/10	1/3	1	3	10
0.25	2.8	3.0	2.9	2.9	2.9	6.0	5.8	5.4	4.9	4.2	1.1	1.2	0.8	1.0	0.5	1.0	0.3	1.1	0.1	1.1
0.5	2.8	2.9	2.6	2.3	1.8	5.9	5.6	5.0	4.1	3.0	1.1	1.2	0.8	1.1	0.7	1.4	0.4	1.7	0.2	2.7
1	2.7	2.6	2.1	1.5	0.9	5.8	5.3	4.3	3.0	1.8	1.1	1.2	1.0	1.3	1.0	2.0	1.0	4.0	1.1	12.
2	2.5	2.4	1.8	1.2	0.7	5.5	4.8	3.7	2.6	1.5	1.3	1.4	1.2	1.6	1.4	1.7	1.6	6.2	1.8	20.
4	2.4	2.3	1.7	1.1	0.6	5.4	4.6	3.6	2.4	1.4	1.4	1.6	1.3	1.8	1.5	3.1	1.8	7.1	2.2	24.
8	2.4	2.2	1.7	1.1	0.6	5.2	4.5	3.5	2.3	1.3	1.4	1.6	1.4	1.8	1.6	3.2	1.9	7.5	2.5	27.
16	2.3	2.1	1.6	1.1	0.6	5.2	4.5	3.4	2.3	1.3	1.5	1.6	1.4	1.9	1.7	3.3	2.0	7.8	2.3	25.

Table 4 Columns 2 to 6 give the ratio of the core-radii of both components in our model, column 7 gives it in the Test-Component model (see text). Columns 8 to 12 give the ratio of the free-free core radius (as defined by Lea 1973) to the visible core radius; column 13 gives it in the TC model.

η α	1/10	1/3	$1_{cb}/l_{ca}$	3	10	TC	1/10	1/3	$1_{ff}/l_{ca}$	3	10	TC
0.25	0.3	0.3	0.3	0.2	0.1	0.4	0.2	0.2	0.2	0.1	0.1	.26
0.50	0.5	0.5	0.5	0.4	0.3	0.5	0.4	0.3	0.3	0.3	0.2	.4
1	1.0	1.0	1.0	1.0	1.0	1.0	0.6	0.6	0.6	0.6	0.6	.5
2	3.2	2.4	2.0	1.9	1.8	29.	1.0	1.0	1.0	1.0	1.0	10
4	7.9	4.6	3.6	3.0	2.8	900.	2.2	1.8	1.7	1.6	1.6	29.
8	12.	7.1	5.3	4.5	4.4	1200.	4.7	3.2	2.6	2.3	2.4	900.
16	16.	10.	7.4	6.3	6.0	1300.	8.0	5.2	4.0	3.5	3.3	1200.

Table 5 Columns 2 to 6 and 7 to 11 give respectively the dimensionless mass of invisible component and the ratio of both masses within the invisible spherical core r_{cb} . Columns 12 to 16 give the dimensionless free-free luminosity L_{ff}^* . Dimensionless quantities are related to the real ones through relations such as Equation (6) and:

$$M_i(r)/M_i^*(s) = \beta v_a^2 / 12\pi G, \quad i = a, b.$$

η α	$M_b^*(s_{cb})$					$M_b^*/M_a^*(s_{cb})$					L_{ff}^*				
	1/10	1/3	1	3	10	1/10	1/3	1	3	10	1/10	1/3	1	3	10
0.25	0.28	0.71	1.4	1.7	1.4	0.07	0.25	0.71	2.1	6.8	0.02	0.17	0.92	3.4	9.6
0.5	2.2	2.6	5.0	59	4.3	0.20	0.26	0.77	2.3	7.7	0.09	0.78	4.2	15.	41.
1	4.5	11.	18.	20.	14.	0.10	0.33	1.0	3.0	10.	0.55	4.8	23.	74.	180.
2	67.	80.	83.	68.	43.	0.30	0.74	1.9	5.5	17.	15.	52.	150.	360.	770.
4	660.	460.	320.	210.	120.	2.0	3.1	5.9	14.	41.	150.	370.	800.	1.6×10^3	3.2×10^3
8	3300.	1800.	1100.	670.	360.	11.	13.	22.	47.	130.	920.	1.9×10^3	3.7×10^3	6.9×10^3	1.3×10^4
16	9800.	5600.	3200.	1900.	1020.	37.	45.	69.	150.	400.	4.5×10^3	8.5×10^3	1.6×10^4	2.8×10^4	5.3×10^4

Table 6 Columns 2 to 11 give respectively for each component the dimensionless masses (as defined in Equation (9)) in the cylinders which project within both core radii. Columns 12 to 16 give the ratio of both masses within the cylindrical invisible core.

η	$M_a^*(l_{ca})$					$M_b^*(l_{cb})$					$M_b^*/M_a^*(l_{cb})$				
	1/10	1/3	1	3	10	1/10	1/3	1	3	10	1/10	1/3	1	3	10
0.25	110	102.	94.	79.	79.	5.1	1.4	2.7	3.4	2.9	.03	0.09	0.24	0.59	1.4
0.5	110	90.	69.	44.	22.	1.8	5.0	9.6	12.	9.5	.05	0.15	0.41	1.1	3.1
1	96	71.	39.	14.	3.0	9.6	24.	39.	43.	30.	0.10	0.33	1.0	3.0	10.
2	80	55.	25.	7.8	1.6	190.	210.	190.	150.	92.	.7	1.5	3.5	9.3	30.
4	73	47.	20	6.6	1.3	2000.	1100.	730.	450.	270.	6.5	7.9	14.	30.	96.
8	67	43.	19,	6.0	1.2	8100.	4100.	2400.	1400.	770.	3.1	33.	52.	110.	310.
16	69	42.	18.	5.6	1.1	23000	12000	69000.	4100.	2300.	9.7	110.	160.	340.	1000.

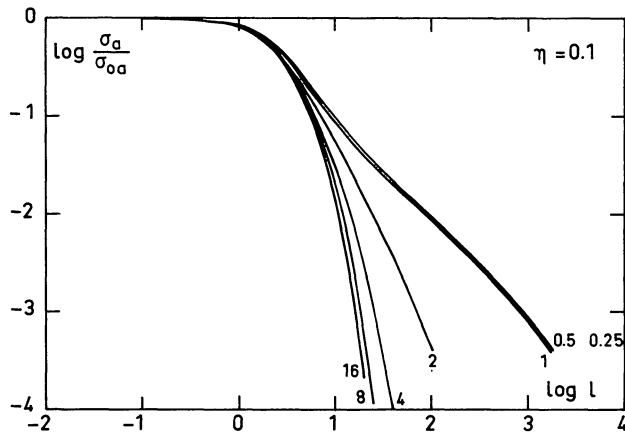


Figure 1 Surface density profiles of the visible component. The surface density is normalized to its central value. The radial distance is given in units of the *structural index* β defined in section II. The ratio of central densities is $\eta=1/10$, the values of α are given on the corresponding profiles.

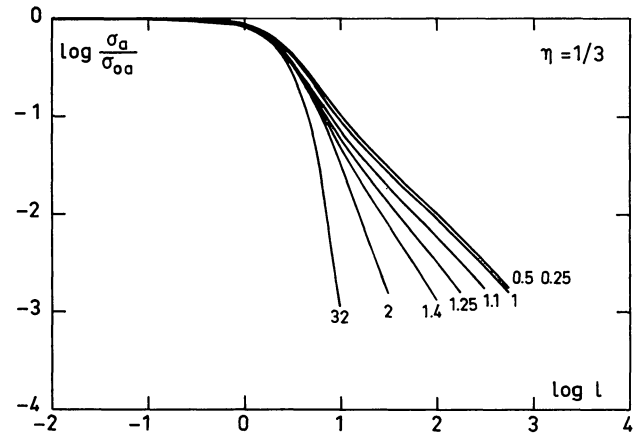


Figure 2 Same as figure 1 for $\eta=1/3$.

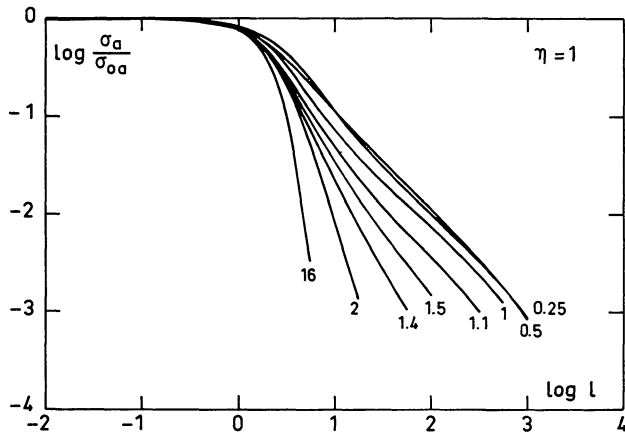


Figure 3 Same as figure 1 for $\eta=1$.

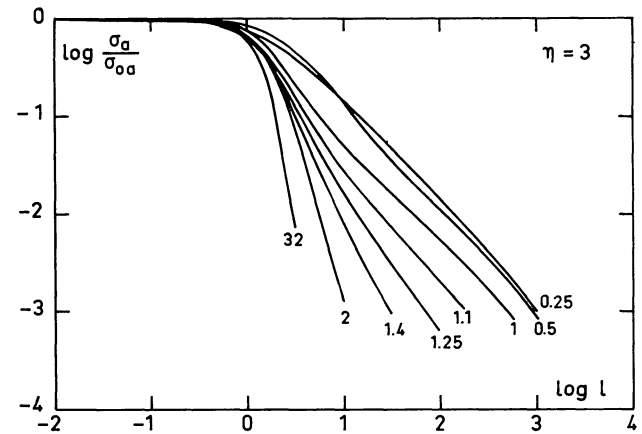


Figure 4 Same as figure 1 for $\eta=3$.

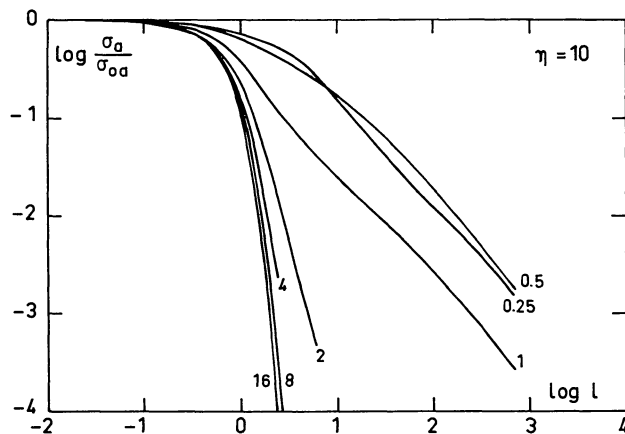


Figure 5 Same as figure 1 for $\eta=10$.

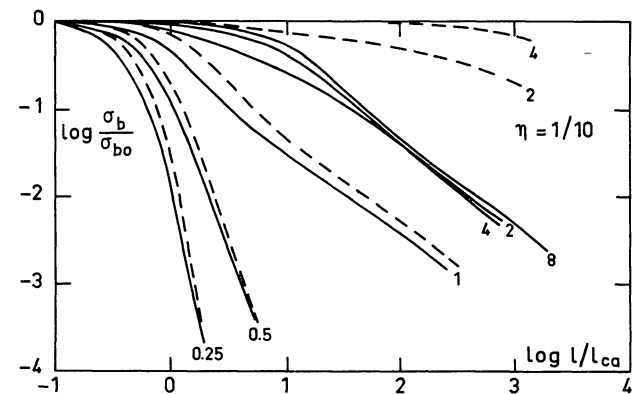


Figure 6 Surface density profiles of the invisible component. The surface density is normalized to its central value. The radial distance is measured in units of the *visible core radius*. The ratio of both central mass densities is $\eta=1/10$, the values of α are given on the corresponding profiles. Dotted profiles correspond to TC model.

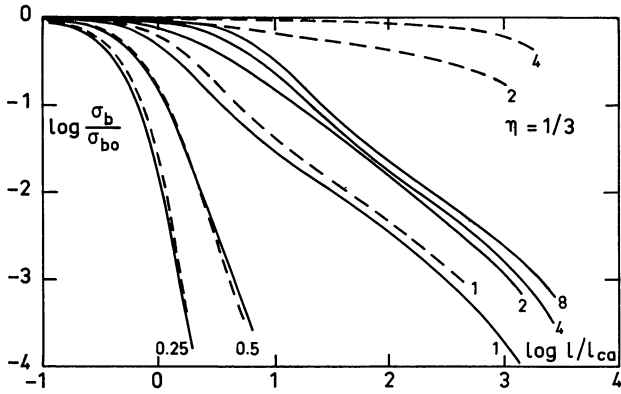
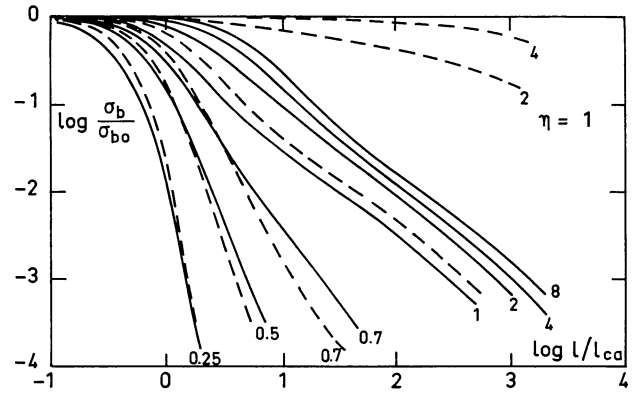
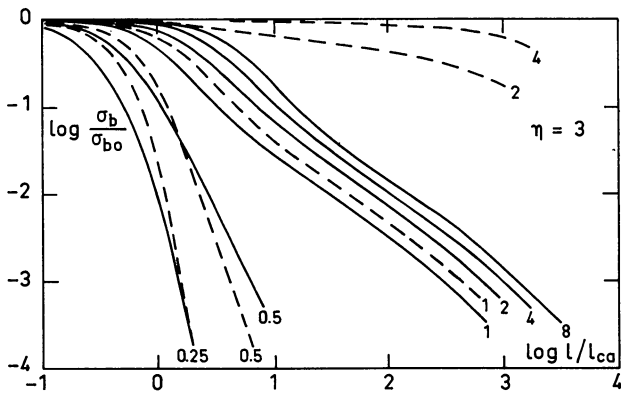
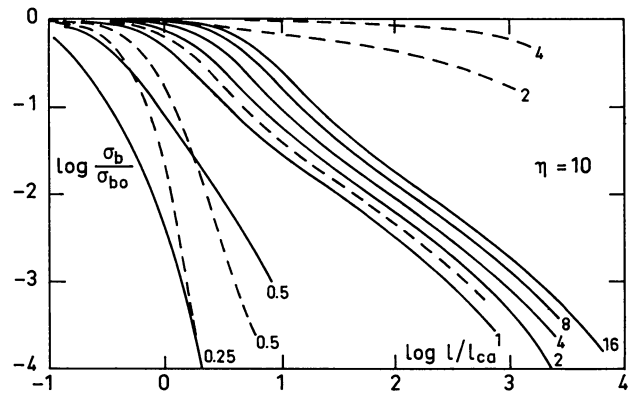
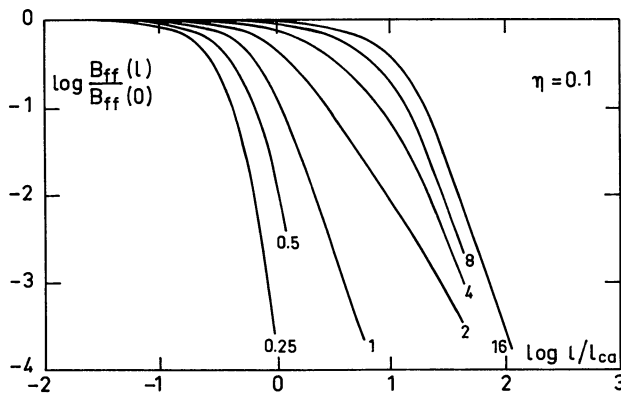
Figure 7 Same as figure 6 for $\eta = 1/3$.Figure 8 Same as figure 6 for $\eta = 1$.Figure 9 Same as figure 6 for $\eta = 3$.Figure 10 Same as figure 6 for $\eta = 10$.

Figure 11 Brightness density profiles for free-free emission of the second component, normalized to its central value. The radial distance is measured in units of the *visible core radius*. The ratio of both central mass densities is $\eta = 1/10$. The values of α are given on the corresponding profiles. Dotted profiles correspond to TC model.

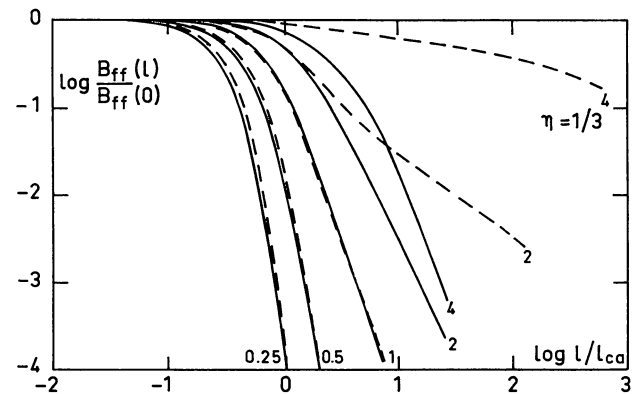
Figure 12 Same as figure 11 for $\eta = 1/3$.

Table 1 (continued)

ETA = 10.30 ALPHA = 1.00										ETA = 10.30 ALPHA = 16.00									
LOG S	PS1	RHO A	RHO B	M A	M B	M	L X	LOG S	PS1	RHO A	RHO B	M A	M B	M	L X				
1.0	3.103E+31	0.1130E+32	0.0	0.0	0.0	0.0	0.0	-2.60	3.0	0.100E+01	0.113E+32	3.0	0.0	0.0	0.0				
1.01	3.117E+31	0.1135E+32	0.0	0.0	0.0	0.0	0.0	-1.75	0.100E+01	0.1135E+32	3.0	0.0	0.0	0.0	0.0				
1.02	3.131E+31	0.1140E+32	0.0	0.0	0.0	0.0	0.0	-1.15	0.100E+01	0.1140E+32	3.0	0.0	0.0	0.0	0.0				
1.03	3.145E+31	0.1145E+32	0.0	0.0	0.0	0.0	0.0	-0.85	0.100E+01	0.1145E+32	3.0	0.0	0.0	0.0	0.0				
1.04	3.159E+31	0.1150E+32	0.0	0.0	0.0	0.0	0.0	-0.75	0.100E+01	0.1150E+32	3.0	0.0	0.0	0.0	0.0				
1.05	3.173E+31	0.1155E+32	0.0	0.0	0.0	0.0	0.0	-0.70	0.100E+01	0.1155E+32	3.0	0.0	0.0	0.0	0.0				
1.06	3.187E+31	0.1160E+32	0.0	0.0	0.0	0.0	0.0	-0.68	0.100E+01	0.1160E+32	3.0	0.0	0.0	0.0	0.0				
1.07	3.201E+31	0.1165E+32	0.0	0.0	0.0	0.0	0.0	-0.67	0.100E+01	0.1165E+32	3.0	0.0	0.0	0.0	0.0				
1.08	3.215E+31	0.1170E+32	0.0	0.0	0.0	0.0	0.0	-0.66	0.100E+01	0.1170E+32	3.0	0.0	0.0	0.0	0.0				
1.09	3.229E+31	0.1175E+32	0.0	0.0	0.0	0.0	0.0	-0.65	0.100E+01	0.1175E+32	3.0	0.0	0.0	0.0	0.0				
1.10	3.243E+31	0.1180E+32	0.0	0.0	0.0	0.0	0.0	-0.64	0.100E+01	0.1180E+32	3.0	0.0	0.0	0.0	0.0				
1.11	3.257E+31	0.1185E+32	0.0	0.0	0.0	0.0	0.0	-0.63	0.100E+01	0.1185E+32	3.0	0.0	0.0	0.0	0.0				
1.12	3.271E+31	0.1190E+32	0.0	0.0	0.0	0.0	0.0	-0.62	0.100E+01	0.1190E+32	3.0	0.0	0.0	0.0	0.0				
1.13	3.285E+31	0.1195E+32	0.0	0.0	0.0	0.0	0.0	-0.61	0.100E+01	0.1195E+32	3.0	0.0	0.0	0.0	0.0				
1.14	3.299E+31	0.1200E+32	0.0	0.0	0.0	0.0	0.0	-0.60	0.100E+01	0.1200E+32	3.0	0.0	0.0	0.0	0.0				
1.15	3.313E+31	0.1205E+32	0.0	0.0	0.0	0.0	0.0	-0.59	0.100E+01	0.1205E+32	3.0	0.0	0.0	0.0	0.0				
1.16	3.327E+31	0.1210E+32	0.0	0.0	0.0	0.0	0.0	-0.58	0.100E+01	0.1210E+32	3.0	0.0	0.0	0.0	0.0				
1.17	3.341E+31	0.1215E+32	0.0	0.0	0.0	0.0	0.0	-0.57	0.100E+01	0.1215E+32	3.0	0.0	0.0	0.0	0.0				
1.18	3.355E+31	0.1220E+32	0.0	0.0	0.0	0.0	0.0	-0.56	0.100E+01	0.1220E+32	3.0	0.0	0.0	0.0	0.0				
1.19	3.369E+31	0.1225E+32	0.0	0.0	0.0	0.0	0.0	-0.55	0.100E+01	0.1225E+32	3.0	0.0	0.0	0.0	0.0				
1.20	3.383E+31	0.1230E+32	0.0	0.0	0.0	0.0	0.0	-0.54	0.100E+01	0.1230E+32	3.0	0.0	0.0	0.0	0.0				
1.21	3.397E+31	0.1235E+32	0.0	0.0	0.0	0.0	0.0	-0.53	0.100E+01	0.1235E+32	3.0	0.0	0.0	0.0	0.0				
1.22	3.411E+31	0.1240E+32	0.0	0.0	0.0	0.0	0.0	-0.52	0.100E+01	0.1240E+32	3.0	0.0	0.0	0.0	0.0				
1.23	3.425E+31	0.1245E+32	0.0	0.0	0.0	0.0	0.0	-0.51	0.100E+01	0.1245E+32	3.0	0.0	0.0	0.0	0.0				
1.24	3.439E+31	0.1250E+32	0.0	0.0	0.0	0.0	0.0	-0.50	0.100E+01	0.1250E+32	3.0	0.0	0.0	0.0	0.0				
1.25	3.453E+31	0.1255E+32	0.0	0.0	0.0	0.0	0.0	-0.49	0.100E+01	0.1255E+32	3.0	0.0	0.0	0.0	0.0				
1.26	3.467E+31	0.1260E+32	0.0	0.0	0.0	0.0	0.0	-0.48	0.100E+01	0.1260E+32	3.0	0.0	0.0	0.0	0.0				
1.27	3.481E+31	0.1265E+32	0.0	0.0	0.0	0.0	0.0	-0.47	0.100E+01	0.1265E+32	3.0	0.0	0.0	0.0	0.0				
1.28	3.495E+31	0.1270E+32	0.0	0.0	0.0	0.0	0.0	-0.46	0.100E+01	0.1270E+32	3.0	0.0	0.0	0.0	0.0				
1.29	3.509E+31	0.1275E+32	0.0	0.0	0.0	0.0	0.0	-0.45	0.100E+01	0.1275E+32	3.0	0.0	0.0	0.0	0.0				
1.30	3.523E+31	0.1280E+32	0.0	0.0	0.0	0.0	0.0	-0.44	0.100E+01	0.1280E+32	3.0	0.0	0.0	0.0	0.0				
1.31	3.537E+31	0.1285E+32	0.0	0.0	0.0	0.0	0.0	-0.43	0.100E+01	0.1285E+32	3.0	0.0	0.0	0.0	0.0				
1.32	3.551E+31	0.1290E+32	0.0	0.0	0.0	0.0	0.0	-0.42	0.100E+01	0.1290E+32	3.0	0.0	0.0	0.0	0.0				
1.33	3.565E+31	0.1295E+32	0.0	0.0	0.0	0.0	0.0	-0.41	0.100E+01	0.1295E+32	3.0	0.0	0.0	0.0	0.0				
1.34	3.579E+31	0.1300E+32	0.0	0.0	0.0	0.0	0.0	-0.40	0.100E+01	0.1300E+32	3.0	0.0	0.0	0.0	0.0				
1.35	3.593E+31	0.1305E+32	0.0	0.0	0.0	0.0	0.0	-0.39	0.100E+01	0.1305E+32	3.0	0.0	0.0	0.0	0.0				
1.36	3.607E+31	0.1310E+32	0.0	0.0	0.0	0.0	0.0	-0.38	0.100E+01	0.1310E+32	3.0	0.0	0.0	0.0	0.0				
1.37	3.621E+31	0.1315E+32	0.0	0.0	0.0	0.0	0.0	-0.37	0.100E+01	0.1315E+32	3.0	0.0	0.0	0.0	0.0				
1.38	3.635E+31	0.1320E+32	0.0	0.0	0.0	0.0	0.0	-0.36	0.100E+01	0.1320E+32	3.0	0.0	0.0	0.0	0.0				
1.39	3.649E+31	0.1325E+32	0.0	0.0	0.0	0.0	0.0	-0.35	0.100E+01	0.1325E+32	3.0	0.0	0.0	0.0	0.0				
1.40	3.663E+31	0.1330E+32	0.0	0.0	0.0	0.0	0.0	-0.34	0.100E+01	0.1330E+32	3.0	0.0	0.0	0.0	0.0				
1.41	3.677E+31	0.1335E+32	0.0	0.0	0.0	0.0	0.0	-0.33	0.100E+01	0.1335E+32	3.0	0.0	0.0	0.0	0.0				
1.42	3.691E+31	0.1340E+32	0.0	0.0	0.0	0.0	0.0	-0.32	0.100E+01	0.1340E+32	3.0	0.0	0.0	0.0	0.0				
1.43	3.705E+31	0.1345E+32	0.0	0.0	0.0	0.0	0.0	-0.31	0.100E+01	0.1345E+32	3.0	0.0	0.0	0.0	0.0				
1.44	3.719E+31	0.1350E+32	0.0	0.0	0.0	0.0	0.0	-0.30	0.100E+01	0.1350E+32	3.0	0.0	0.0	0.0	0.0				
1.45	3.733E+31	0.1355E+32	0.0	0.0	0.0	0.0	0.0	-0.29	0.100E+01	0.1355E+32	3.0	0.0	0.0	0.0	0.0				
1.46	3.747E+31	0.1360E+32	0.0	0.0	0.0	0.0	0.0	-0.28	0.100E+01	0.1360E+32	3.0	0.0	0.0	0.0	0.0				
1.47	3.761E+31	0.1365E+32	0.0	0.0	0.0	0.0	0.0	-0.27	0.100E+01	0.1365E+32	3.0	0.0	0.0	0.0	0.0				
1.48	3.775E+31	0.1370E+32	0.0	0.0	0.0	0.0	0.0	-0.26	0.100E+01	0.1370E+32	3.0	0.0	0.0	0.0	0.0				
1.49	3.789E+31	0.1375E+32	0.0	0.0	0.0	0.0	0.0	-0.25	0.100E+01	0.1375E+32	3.0	0.0	0.0	0.0	0.0				
1.50	3.803E+31	0.1380E+32	0.0	0.0	0.0	0.0	0.0	-0.24	0.100E+01	0.1380E+32	3.0	0.0	0.0	0.0	0.0				
1.51	3.817E+31	0.1385E+32	0.0	0.0	0.0	0.0	0.0	-0.23	0.100E+01	0.1385E+32	3.0	0.0	0.0	0.0	0.0				
1.52	3.831E+31	0.1390E+32	0.0	0.0	0.0	0.0	0.0	-0.22	0.100E+01	0.1390E+32	3.0	0.0	0.0	0.0	0.0				
1.53	3.845E+31	0.1395E+32	0.0	0.0	0.0	0.0	0.0	-0.21	0.100E+01	0.1395E+32	3.0	0.0	0.0	0.0	0.0				
1.54	3.859E+31	0.1400E+32	0.0	0.0	0.0	0.0	0.0	-0.20	0.100E+01	0.1400E+32	3.0	0.0	0.0	0.0	0.0				
1.55	3.873E+31	0.1405E+32	0.0	0.0	0.0	0.0	0.0	-0.19	0.100E+01	0.1405E+32	3.0	0.0	0.0	0.0	0.0				
1.56	3.887E+31	0.1410E+32	0.0	0.0	0.0	0.0	0.0	-0.18	0.100E+01	0.1410E+32	3.0	0.0	0.0	0.0	0.0				
1.57	3.901E+31	0.1415E+32	0.0	0.0	0.0	0.0	0.0	-0.17	0.100E+01	0.1415E+32	3.0	0.0	0.0	0.0	0.0				
1.58	3.915E+31	0.1420E+32	0.0	0.0	0.0	0.0	0.0	-0.16	0.100E+01	0.1420E+32	3.0	0.0	0.0	0.0	0.0				
1.59	3.929E+31	0.1425E+32	0.0	0.0	0.0	0.0	0.0	-0.15	0.100E+01	0.1425E+32	3.0	0.0	0.0	0.0	0.0				
1.60	3.943E+31	0.1430E+32	0.0	0.0	0.0	0.0	0.0	-0.14	0.100E+01	0.1430E+32	3.0	0.0	0.0	0.0	0.0				
1.61	3.957E+31	0.1435E+32	0.0	0.0	0.0	0.0	0.0	-0.13	0.100E+01	0.1435E+32	3.0	0.0	0.0	0.0	0.0				
1.62	3.971E+31	0.1440E+32	0.0	0.0	0.0	0.0	0.0	-0.12	0.100E+01	0.1440E+32	3.0	0.0	0.0	0.0	0.0				
1.63	3.985E+31	0.1445E+32	0.0	0.0	0.0	0.0	0.0	-0.11	0.100E+01	0.1445E+32	3.0	0.0	0.0	0.0	0.0				
1.64	3.999E+31	0.1450E+32	0.0	0.0	0.0	0.0	0.0	-0.10	0.100E+01	0.1450E+32	3.0	0.0	0.0	0.0	0.0				
1.65	4.013E+31	0.1455E+32	0.0	0.0	0.0	0.0	0.0	-0.09	0.100E+01	0.1455E+32	3.0	0.0	0.0	0.0	0.0				
1.66	4.027E+31	0.1460E+32	0.0	0.0	0.0	0.0	0.0	-0.08	0.100E+01	0.1460E+32	3.0	0.0	0.0	0.0	0.0				
1.67	4.041E+31	0.1465E+32	0.0	0.0	0.0	0.0	0.0	-0.07	0.100E+01	0.1465E+32	3.0	0.0	0.0	0.0	0.0				
1.68	4.055E+31	0.1470E+32	0.0	0.0	0.0	0.0	0.0	-0.06	0.100E+01	0.1470E+32	3.0	0.0	0.0	0.0	0.0				
1.69	4.069E+31	0.1475E+32	0.0	0.0	0.0	0.0	0.0	-0.05	0.100E+01	0.1475E+32	3.0	0.0	0.0	0.0	0.0				
1.70	4.083E+31	0.1480E+32	0.0	0.0	0.0	0.0	0.0	-0.04	0.100E+01	0.1480E+32	3.0	0.0	0.0	0.0	0.0				
1.71	4.097E+31	0.1485E+32	0.0	0.0	0.0	0.0	0.0	-0.03	0.100E+01	0.1485E+32	3.0	0.0	0.0	0.0	0.0				
1.72	4.111E+31	0.1490E+32	0.0	0.0	0.0	0.0	0.0	-0.02	0.100E+01	0.1490E+32	3.0	0.0	0.0	0.0	0.0				
1.73	4.125E+31	0.1495E+32	0.0	0.0	0.0	0.0	0.0	-0.01	0.100E+01	0.1495E+32	3.0	0.0	0.0	0.0	0.0				
1.74	4.139E+31	0.1500E+32	0.0	0.0	0.0	0.0	0.0	0.0	0.100E+01	0									

Table 1 (continued)

Table with 16 columns: LCG S, PSI, RHO A, RHO B, M A, M B, M, L X, LCG S, PSI, RHO A, RHO B, M A, M B, M, L X. Parameters: ETA = 3.00, ALPHA = 2.00, ETA = 1.00, ALPHA = 0.25.

Table with 16 columns: LCG S, PSI, RHO A, RHO B, M A, M B, M, L X, LCG S, PSI, RHO A, RHO B, M A, M B, M, L X. Parameters: ETA = 3.00, ALPHA = 4.00, ETA = 1.00, ALPHA = 0.50.

Table with 16 columns: LCG S, PSI, RHO A, RHO B, M A, M B, M, L X, LCG S, PSI, RHO A, RHO B, M A, M B, M, L X. Parameters: ETA = 3.00, ALPHA = 6.00, ETA = 1.00, ALPHA = 1.00.

Table with 16 columns: LCG S, PSI, RHO A, RHO B, M A, M B, M, L X, LCG S, PSI, RHO A, RHO B, M A, M B, M, L X. Parameters: ETA = 3.00, ALPHA = 16.00, ETA = 1.00, ALPHA = 2.00.

Two Component Emden Sphere

Table 1 (continued)

Table 1 (continued) - Top section. Parameters: ETA = 0.33, ALPHA = 0.00, ETA = 0.10, ALPHA = 1.00. Columns: LGG 5, PSI, RHO A, RHO B, N A, N B, N, L X, LGG 5, PSI, RHO A, RHO B, N A, N B, N, L X.

Table 1 (continued) - Middle section. Parameters: ETA = 0.33, ALPHA = 16.00, ETA = 0.10, ALPHA = 2.00. Columns: LGG 5, PSI, RHO A, RHO B, N A, N B, N, L X, LGG 5, PSI, RHO A, RHO B, N A, N B, N, L X.

Table 1 (continued) - Bottom section. Parameters: ETA = 3.10, ALPHA = 0.25, ETA = 0.10, ALPHA = 4.00, ETA = 0.10, ALPHA = 0.50, ETA = 3.10, ALPHA = 8.00. Columns: LGG 5, PSI, RHO A, RHO B, N A, N B, N, L X, LGG 5, PSI, RHO A, RHO B, N A, N B, N, L X.

Table 1 (continued)

ETA = 0.10 ALPHA = 15.00

LCG 5	PSI	RHD A	RHD B	M A	M B	F	L X
-2.00	0.0	3.103E+31	0.103E+30	0.0	0.0	0.0	0.0
-1.99	0.21E-36	0.110E+31	0.112E+30	0.27E-38	0.27E-36	0.03E+00	0.030E-04
-1.97	0.230E-34	0.110E+31	0.112E+30	0.104E-34	0.104E-35	0.21E-04	0.212E-06
-1.94	0.63E-34	0.110E+31	0.112E+30	0.17E-34	0.17E-35	0.26E-04	0.262E-05
-1.90	0.143E-23	0.100E+01	0.102E+33	0.138E-33	0.138E-34	0.141E-03	0.141E-05
-1.88	0.202E-33	0.100E+01	0.102E+33	0.110E-33	0.110E-34	0.34E-03	0.34E-04
-1.85	0.331E-23	0.700E+00	0.107E+33	0.740E-33	0.741E-34	0.81E-03	0.206E-04
-1.83	0.041E-23	0.090E+00	0.107E+33	0.176E-33	0.176E-34	0.194E-02	0.795E-04
-1.80	0.179E-22	0.070E+00	0.107E+33	0.418E-32	0.418E-33	0.450E-02	0.107E-03
-1.68	0.201E-22	0.070E+00	0.107E+33	0.001E-32	0.001E-33	0.105E-01	0.397E-03
-0.75	0.574E-22	0.094E+00	0.102E+33	0.235E-31	0.235E-32	0.29E-01	0.942E-03
-0.61	0.102E-21	0.093E+00	0.097E+31	0.03E-31	0.03E-32	0.01E-01	0.223E-02
-0.50	0.133E-21	0.093E+00	0.097E+31	0.131E+00	0.132E-01	0.144E+00	0.524E-02
-0.38	0.32E-21	0.093E+00	0.097E+31	0.308E+00	0.308E-01	0.338E+00	0.123E-01
-0.28	0.07E-21	0.044E+00	0.044E+31	0.720E+00	0.743E-01	0.794E+00	0.207E-01
-0.23	0.103E+00	0.044E+00	0.044E+31	0.169E+00	0.176E+00	0.184E+01	0.701E-01
-0.09	0.17E+00	0.044E+00	0.044E+31	0.377E+00	0.418E+00	0.418E+01	0.163E+00
0.00	0.103E+00	0.044E+00	0.044E+31	0.320E+01	0.482E+00	0.027E+01	0.309E+00
0.05	0.03E+00	0.044E+00	0.044E+31	0.174E+00	0.211E+01	0.197E+00	0.308E+00
0.17	0.017E+00	0.044E+00	0.044E+31	0.139E+02	0.241E+01	0.337E+02	0.209E+01
0.20	0.123E+01	0.031E+31	0.031E+31	0.608E+03	0.645E+02	0.71E+02	0.479E+01
0.62	0.188E+21	0.113E+00	0.049E-11	0.978E+02	0.252E+02	0.127E+03	0.107E+02
0.65	0.205E+31	0.090E-01	0.048E-11	0.142E+03	0.043E+02	0.208E+02	0.239E+02
0.67	0.353E+31	0.270E-01	0.000E-11	0.186E+33	0.150E+03	0.338E+03	0.512E+02
1.00	0.473E+01	0.080E-02	0.074E-11	0.284E+33	0.336E+03	0.505E+03	0.109E+03
1.16	0.623E+01	0.233E-02	0.679E-11	0.249E+33	0.742E+03	0.932E+03	0.228E+03
1.20	0.803E+01	0.070E-02	0.548E-11	0.265E+03	0.101E+04	0.362E+04	0.443E+03
1.30	0.111E+02	0.149E-04	0.438E-11	0.265E+03	0.338E+04	0.362E+04	0.824E+03
1.50	0.104E+02	0.211E-06	0.36E-11	0.063E+03	0.063E+04	0.694E+04	0.147E+04
1.62	0.211E+02	0.361E-77	0.244E-11	0.263E+03	0.124E+05	0.126E+05	0.213E+04
1.70	0.204E+02	0.257E-12	0.19E-11	0.263E+03	0.212E+05	0.214E+05	0.382E+04
1.79	0.388E+02	0.107E-16	0.048E-12	0.263E+03	0.332E+05	0.332E+05	0.346E+04
2.00	0.434E+02	0.102E-21	0.447E-12	0.263E+03	0.463E+05	0.488E+05	0.488E+04
2.12	0.380E+02	0.44E-26	0.223E-12	0.263E+03	0.408E+05	0.408E+05	0.407E+04
2.25	0.0721E+02	0.011E-31	0.111E-12	0.263E+03	0.871E+05	0.874E+05	0.420E+04
2.37	0.038E+02	0.217E-40	0.287E-13	0.263E+03	0.141E+06	0.142E+06	0.433E+04
2.50	0.016E+02	0.41E-56	0.383E-13	0.263E+03	0.112E+06	0.112E+06	0.42E+04
2.62	0.104E+03	0.102E+44	0.134E-03	0.263E+03	0.178E+06	0.178E+06	0.438E+04
2.70	0.111E+03	0.79E+41	0.044E-04	0.263E+03	0.222E+06	0.222E+06	0.438E+04
2.87	0.123E+03	0.046E-03	0.445E-04	0.263E+03	0.292E+06	0.292E+06	0.440E+04
3.00	0.131E+03	0.151E-05	0.281E-04	0.263E+03	0.377E+06	0.377E+06	0.441E+04
3.12	0.139E+03	0.033E-03	0.164E-04	0.263E+03	0.487E+06	0.487E+06	0.442E+04
3.25	0.148E+03	0.051E-04	0.993E-05	0.263E+03	0.664E+06	0.664E+06	0.443E+04
3.37	0.157E+03	0.113E-07	0.593E-05	0.263E+03	0.865E+06	0.865E+06	0.444E+04
3.50	0.162E+03	0.0	0.325E-05	0.263E+03	0.122E+07	0.122E+07	0.444E+04
3.62	0.174E+03	0.3	0.157E-05	0.263E+03	0.166E+07	0.166E+07	0.444E+04
3.75	0.181E+03	0.3	0.126E-05	0.263E+03	0.224E+07	0.224E+07	0.444E+04
3.87	0.192E+03	0.3	0.97E-06	0.263E+03	0.304E+07	0.304E+07	0.444E+04
4.00	0.203E+03	0.3	0.33E-06	0.263E+03	0.409E+07	0.409E+07	0.444E+04
4.12	0.211E+03	0.3	0.183E-06	0.263E+03	0.546E+07	0.546E+07	0.444E+04
4.25	0.221E+03	0.3	0.113E-06	0.263E+03	0.731E+07	0.731E+07	0.445E+04